Journal of Loss Prevention in the Process Industries 85 (2023) 105176

Contents lists available at ScienceDirect

Journal of Loss Prevention in the Process Industries

journal homepage: www.elsevier.com/locate/jlp

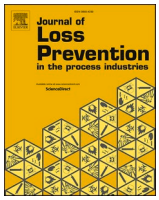

Estimation of burst pressure of pipelines with interacting corrosion clusters based on machine learning models

Abraham Mensah [a,b], Srinivas Sriramula [c,*]

[a] National Decommissioning Centre, School of Engineering, University of Aberdeen, Aberdeen, Scotland, UK
[b] Ghana National Gas Company (GNGC), Accra, Ghana
[c] School of Engineering, University of Aberdeen, Aberdeen, Scotland, UK

ARTICLE INFO

Keywords:
Pipeline burst pressure
Interacting corrosion clusters
Improved corrosion defect shapes
Finite element methods
Supervised machine learning

ABSTRACT

Pipeline corrosion defects mostly appear in a colony such that they interact to reduce the failure pressure, which is not defined by features of a single corrosion defect. The huge amount of corrosion defects captured by in-line inspection tools including the variability of defect profile in pipelines and the dependence of the reliability assessment on such data pose significant research challenges in performance assurance. This highlights the need for computationally efficient modelling schemes to estimate the burst pressure of pipelines affected by both longitudinal and circumferential interacting corrosion defects. In the present paper, a novel approach is proposed for this purpose by combining supervised machine learning methods with 25 numerical models of corroded pipelines, validated with experimental results available from literature. Additionally, six improved composite defect shapes are proposed, resulting in 150 models to examine the non-linear behaviour of interacting corrosion defects by capturing the real the defect profiles captured by the In-line Inspection tools. The predicted failure pressures from the developed numerical models produced an absolute mean deviation of not exceeding 2.03% and 2.2% from the experimental burst pressure and the modified Mixed Type Interaction approach respectively, better than published results from the literature. Notably, the predicted failure pressures based on real pipeline data, infused with the generated artificial neural networks and non-linear regression models provide a total mean deviation of 3.1% and 7.3% respectively, thereby providing a path for effective maintenance planning.

1. Introduction

Carbon steel pipelines provide the safest and economic mode of transportation for hydrocarbon fluids. Nevertheless, these pipelines are susceptible to internal and external metal loss defects, which usually occur in a cluster. This results in reduction of the pipe wall thickness and the associated tensile and compressive strength capacity that can render it unfit for purpose at the corroded area due to stress concentration, resulting in loss of containment or rupture (ASME B31G, 2012; Benjamin et al., 2007). The pipeline incident statistics compiled by the European Gas Pipeline Incident Data Group covering a period from 1970 to 2019 and similar information from the United States Department of Transportation, Pipeline and Hazardous Materials Safety Administration, and the United Kingdom Onshore Pipelines Operators' Association (UKOPA) depict corrosion as one of the major causes of pipeline incidents and accidents among other causes such as external interference, construction defects and ground movement (EGIG, 2020; U.S. Department of Transport PHMSA, 2020; Lyons et al., 1962). Hence, pipeline operators spend extensive resources on pipeline maintenance activities such as inspections, repairs, and replacement to minimize the consequences associated with product loss, installations, people, and environmental damage. These costs can be reduced as much as possible if decision makers accurately consider the pipeline status using in-line inspection (ILI) information and establish an effective pipeline integrity management system (Amaya-Gó et al., 2016, 2019). Amaya et al. (Amaya-Gó et al., 2019) affirmed the need to accurately evaluate the deterioration effect of corrosion in pipelines to avert high operating costs relating to maintenance activities. The deterministic and probabilistic approaches for the structural integrity assessment of single corrosion defects in pipelines have been well researched in the literature, however, very limited research focused on developing a unified computationally efficient modelling approach to evaluate interacting corrosion defects in pipelines. Multiple corrosion defects in a pipeline are said to be interacting, if the presence of other defect is such that, it further reduces the

* Corresponding author.
E-mail addresses: a.mensah.21@abdn.ac.uk (A. Mensah), s.sriramula@abdn.ac.uk (S. Sriramula).

https://doi.org/10.1016/j.jlp.2023.105176
Received 1 July 2022; Received in revised form 8 September 2023; Accepted 17 September 2023
Available online 19 September 2023

failure pressure of the pipeline and is not controlled by a single, metal loss defect feature (Det Norske Veritas, 2004).

Current studies to consider these effects are mainly limited by the lack of experimentally validated and computationally efficient modelling schemes with high precision of burst pressure prediction. Battelle's research work was limited to single corrosion flaws and did not consider any interacting effect of multiple corrosion defects on the pipeline strength. However, the American Society of Mechanical Engineers (ASME) B31G (ASME B31G, 2012) guidelines outlined minimum guidance on interaction rules and assessment of multiple corrosion that are longitudinally or circumferentially spaced due to limited test data. These guidelines recommended that, all interacting flaws that are more than three multiplied by the pipe wall thickness ($3t$) should be treated as a single composite flaw. To improve on the effectiveness of ASME B31G general guidelines for interacting metal loss flaws, Det Norske Veritas (DNV) used deterministic and probabilistic approaches for the interacting rules and pipeline failure pressure estimates subjected to only internal pressure loadings. DNV considered the maximum operating pressure of a pipeline section with an external diameter (D), treated as a single defect or a composite defect with an assumed rectangular defect shape (RDS) if the minimum corrosion cluster length is $5.0\sqrt{Dt}$ and the minimum overlap for the internal and external corrosion defects is $2.5\sqrt{Dt}$ (Det Norske Veritas, 2004). However, these assessments are conservative in burst pressure prediction of interacting corrosion cluster defects.

Over the past two decades, researchers have adopted finite element methods (FEM), machine learning (ML) and other techniques beyond the complex full-scale burst experiments to improve the understanding of the non-linear behaviour of interacting multiple metal loss defects in pipelines. Studies by Silva et al. (2007) used artificial neural networks (ANN) to improve the accuracy of interaction rules and estimation of reduced pipeline burst pressure beyond the DNV-Recommended Practice (RP)-F101 criteria. However, they could not validate their works with real burst test data due to limited information on interacting defects and did not consider the variations relating to the defect profile (Silva et al., 2007). Furthermore, Huang et al. (2022) highlighted, among other contributing factors, the shape of the metal loss defect as a determinant in the accurate prediction of failure pressure for corroded pipelines with dent-corrosion defects. The configuration of longitudinal and circumferentially aligned metal loss flaws and geometry of defect considered were ideal and rectangular shaped respectively, which fail to mirror the practical irregular variations in pipeline corrosion profiles.

Notably, the two sets of full-scale burst tests by Benjamin et al., 2007, 2016a, 2016b under the Mixed Type Interaction (MTI) Joint Industry Project comprised of 30 pressure vessels containing single, multiple machined corrosion defects and corrosion free test samples. The development of the MTI approach (Benjamin et al., 2007) used 12 test samples from the first set of experiments containing multiple machined corrosion defects instead of a pair of defects, as considered by earlier researchers. This improved the integrity assessment of interacting defects with the same depth, giving rise to a mean deviation of about 3.7% to the experimental burst pressure. However, it is worth noting that the experimental sample size with identical depth of ideal RDS was not large enough to support a comprehensive framework for assessment of interacting corrosion. The application of Machine Learning (ML) approaches to pipeline integrity assessments offers an increase in prediction accuracy and reduces the simulation time to discover the non-linear patterns. Mazumder et al. (2021) employed ML algorithms to investigate the deterministic and probabilistic failure pressure of a pipeline with corrosion growth rate for single defect and demonstrated the ability of ML for accurate and faster pipeline integrity assessment than a physics-based process. A decade after the research by Silva et al. (2007) which was not validated due to lack of full-scale test results, Xu et al. (2017) used numerical methods and ANN to predict pipeline failure pressure and interacting rules for a small sample size of multiple pipeline corrosion defects. It was observed that the results from the FEM with rectangular shaped metal loss defects were close to the considered experimental data of American Petroleum Institute (API) 5L ×80, but this study did not account for the variations in defect profile and the corrosion clusters had the same depth. However, the variability in defect geometry affects the integrity of corroded pipelines (Wang et al., 2023). In order to better understand the behaviour of corroded pipelines using machine learning models, Lu et al. (2022) effectively created a framework to increase the prediction accuracy of the maximum metal loss depth of corroded pipelines throughout the operational time. The pipeline failure, however, may not only be influenced by the maximum pitting depth but also by the interacting corrosion cluster features, including the defect geometry, due to the non-linear behaviour of the interacting corrosion cluster defects in pipelines. A recent paper by Lo et al. (2021) confirms the low level of accuracy of existing approaches for burst pressure prediction of corroded pipelines with interacting corrosion cluster and the need for computationally efficient modelling schemes (CEMS).

Considering the above limitations of existing research, this paper proposes numerical approach coupled with Non-Linear Regression models (NLRM) and ANN models incorporating the RDS and the improved corrosion defect shapes to develop computationally efficient models. The finite element analysis performed in this study offers the needed advantage of modelling and examining the burst pressure of corroded pipelines with the proposed improved corrosion defect shapes, which are not available in the literature. This is considered after an acceptable numerical model with rectangular-shaped interacting corrosion cluster has been achieved. The numerical model with a rectangular-shaped interacting corrosion cluster is validated with the experimental burst pressure data available in the published literature. Furthermore, the numerical models with the improved corrosion defect shapes are validated with the modified MTI burst pressures by incorporating the proposed defect shape factors. The present work considers experimental data (25 test samples) from MTI experimental database of interacting corrosion colonies, and uses trained ML weights and biases to improve the accuracy and reduce the computational time for integrity evaluation of interacting corrosion defects in pipelines subjected to internal pressure. as illustrated in Fig. 1. Additionally, the variability of the profile other than the RDS for the interacting corrosion colony captured by a typical magnetic flux leakage (MFL) ILI tool on real pipelines is explored by considering improved defect shapes to provide a pathway for rational decision making relating to maintenance planning and risk management.

2. Modelling parameters based on experimental observations (from literature) and real inspection data

The numerical models and supervised ML models are developed based on the published MTI full-scale burst pressure experiments and anonymized field ILI information. Numerical models of 25 different configurations of interacting corrosion clusters from the MTI full-scale burst test samples are developed and examined. The predicted burst pressure results from the numerical models including the essential pipe and metal loss defect geometric, and material properties are used to derive ML models which are applied on real ILI data to predict the burst pressure.

MTI's burst pressure database on interacting pipeline metal loss defects stems from two separate experiments to understand the behaviour of longitudinal and circumferential interacting corrosion defects in pipelines subjected to internal pressure loadings (Benjamin et al., 2007, 2016b). The first test considered twelve test samples of longitudinal welded pipes made up of API 5L ×80 Carbon steel with three different material properties in terms of the yield and tensile strength capacity. The twelve samples comprised of one defect free pipe, two pipes with single metal loss defects and nine spool pieces containing interacting corrosion defect clusters. The corrosion clusters had varying configuration of defect colonies from two to nine and had the same defect depth.

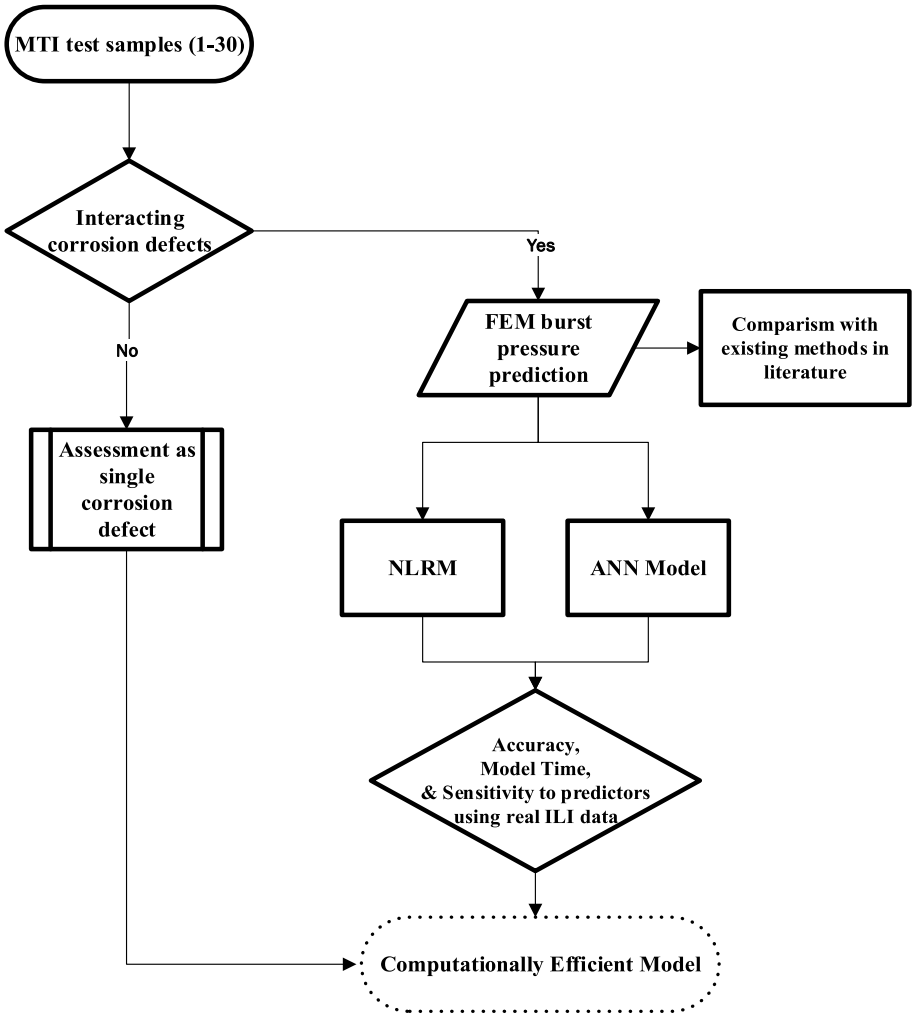

Fig. 1. Flowchart of CEMS for evaluating pipelines with interacting corrosion cluster defects.

The pipe spool piece had a length from 1.7m to 1.9m with varying machined rectangular defects of defect depth to thickness ratio (d/t) between 0.460 and 0.665. The second set of tests were conducted with 18 pipe test samples that contained two pipes with single defect, six pipes with single patch colonies and ten pipes with multiple patch colonies mimicking realistic interacting corrosion in pipelines. The API 5L ×70 carbon steel pipe had five different material properties and the effective defect cluster depth to pipe thickness ratio (d_c/t) varied between 0.390 and 0.630. The key geometric and material properties used in the finite element and machine learning modelling are shown in Table 1.

Table 1
Geometric and material properties for FEM and ML Models (Benjamin et al., 2007, 2016b).

Geometric and Material Properties (Units)	Values
Pipe Diameter, D (mm)	457.0, 458.8, 459.4, 458.6
Pipe wall thickness, t (mm)	7.93, 7.90, 7.91, 7.92, 8.01, 8.10
Tensile strength, UTS (MPa)	684, 698, 728, 731, 732, 739, 748, 773
Yield Strength, SMYS (MPa)	556, 580, 589, 601, 639, 652, 654, 662
Modulus of elasticity, E (GPa)	210
Poisson's ratio, v	0.3
Number of corrosion cluster per test sample	2, 3, 4, 5, 6, 7, 8, 9, 10
Effective defect depth to wall thickness ratio, d_c/t	0.39, 0.47, 0.48, 0.58, 0.60, 0.61, 0.62, 0.63, 0.65, 0.66, 0.67, 0.69
Absolute defect longitudinal spacing, S_L (mm)	9.50, 9.88, 10.00, 19.84, 19.98, 20, 20.06, 20.40, 20.50, 30.00, 39.60
Absolute defect circumferential spacing, S_C (mm)	9.60, 9.88, 9.99, 10.00, 10.01, 10.03, 19.84, 20.00, 30.00, 31.90

A typical observation set from an anonymized MFL ILI data on a 110 km pipeline, highlighting the distribution of internal and external corrosion defects including manufacturing defects as illustrated in Fig. 2 is used to check the performance of the generated NLRM and ANN models. It is observed that the pipeline has sparsely distributed manufacturing defects, limited external corrosion defects but contains more internal corrosion defects, which are clustered especially in the first 30 km span. The ILI results provide the specification of the MFL tool, operating conditions of the intelligent pig and the allowable operating tolerances. The defect sizes in terms of defect length, depth, and width assuming an RDS as the worst case of metal degradation shape, circumferential location, and distance of anomalies to the nearest girth weld, including pitting and clustered metal loss defects detected by the MFL pig are also provided. For this research, 15 severe corrosion cluster defect areas (CCDA) are selected to assess the performance of the produced NLRM and ANN models.

3. Improved corrosion defect shapes

Advances in in-line inspection tools to capture the actual profile of corrosion defects as highlighted by Ma et al. (2021) is a step in the right direction to reduce the variations related to the defect shapes used in integrity and reliability assessment. Hence, there is a need to employ

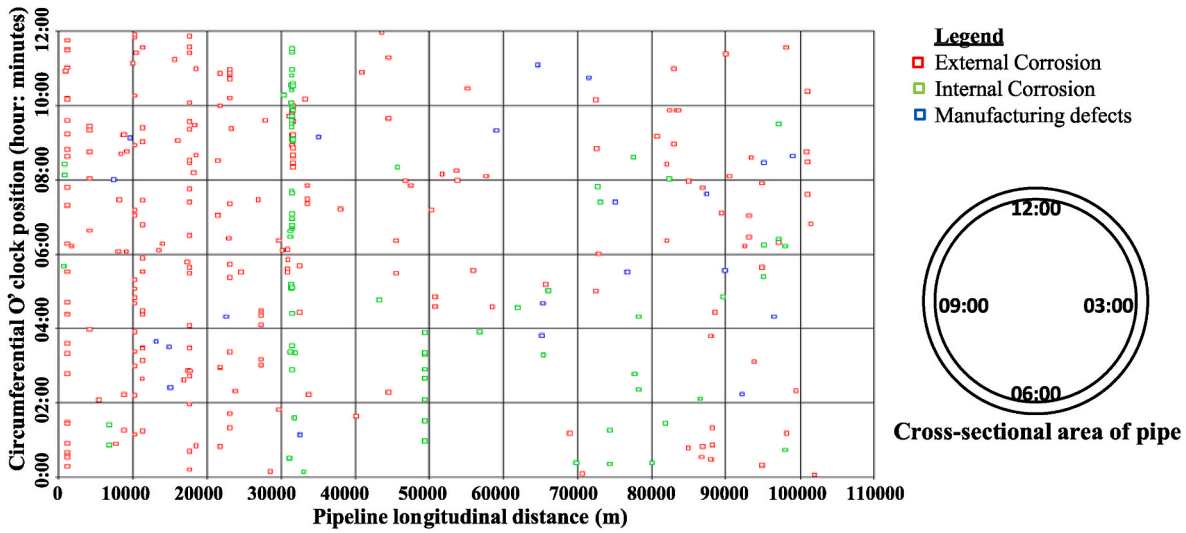

Fig. 2. Typical distribution of internal and external corrosion defects in a pipeline from an MFL inspection tool.

improved metal loss defect shapes to cater for the uncertainties of the defect shapes captured by infield intelligent pigging tool to investigate the non-linear behavior of multiple interacting corrosion defects. In this paper, improved defect shapes beyond the RDS used by MTI and ILI information are considered to address the irregular nature of the profile of interacting corrosion cluster. A number of pipeline corrosion defect shapes have been considered to estimate the remaining static and dynamic strength of pipelines. The American Gas Association and the ASME used the V- notch and rectangular defect shapes to conduct pipeline burst experiments due to the ease of defect creation. The need to reduce the conservatism in integrity assessments resulted in the use of an effective area in the Remaining Strength of Corroded Pipe (RSTRENG) method, 66.67% of metal loss area in AMSE B31G assessment, and 85% of metal loss area in modified B31G defect evaluation method. This was evidenced by the shape factors of 2/3 and 0.85 in the pipeline burst pressure formulae and parabolic defect geometry proposed by O'Grady et al. (ASME B31G, 2012; Cosham et al., 2007; Grady et al., 1992a; Grady et al., 1992b). Table 2 highlights the different metal loss defect shapes considered by several researchers as highlighted in a recent review of pipeline defect assessment by Qin and Cheng (2021) to evaluate single and multiple defects.

In this paper, improved defect shapes of constant volumetric or cross-sectional area ratio to the equivalent RDS are proposed to capture the real defect characteristics effectively. The existing defect shapes such as rectangular, parabolic (PS), and proposed defects shapes such as the semi-elliptical rectangular composite shapes (SERCS), *n*th-stair symmetric complex shape (EnSSC), Pent-symmetric complex shape (PSCS) shown in Fig. 3 are investigated to ascertain the quantum of effect on the pipeline burst pressure. The *n*th -stair symmetric complex defect shape for an equivalent RDS of length L and depth d, has a symmetric n number of steps with a rise of '$d/(n+1)$' and a thread of '$L/(2n)$' as illustrated in Fig. 3.

The constant defect shape factors (S_F) for the considered defect profiles irrespective of the dimensions of the assumed RDS are shown in Table 3. The semi-circular rectangular composite shape (SCRCS) does not have a constant shape factor to an equivalent RDS and hence, could not be considered for this work.

Table 2
Typical corrosion defect shapes.

Defect Shape	Defect Type	Assessment Methods
Parabolic	Single defects	ASME B31G, Chen et al. (Qin and Cheng, 2021)
Rectangular	Single defects	DNV-RP-F101, API RP 579, BS 7910
Elliptical	Single defects	Chen et al. (Qin and Cheng, 2021)
Rectangular	Multiple defects	MTI, Chen et al. (Qin and Cheng, 2021)
Rectangular shallow patch with deep patch	Complex or multiple defects	Sun et al. (Sun et al., 2021)
River bottom irregular shape	Single, complex, or multiple defects	RSTRENG, DNV-RP-F101

4. Numerical and machine learning methods

The finite element burst models of 25 MTI test samples of API 5L ×80 and API 5L ×70 steel pipeline with longitudinally and circumferentially interacting corrosion cluster defects are developed using the RDS and other six improved shapes highlighted in Fig. 3. The predicted failure pressures of the multiple interacting pipeline corrosion defects with RDS are validated with the MTI experimental burst pressures ($P_{b.EXP}$) and those with the proposed shapes are validated using modified MTI burst pressure ($P_{f.ModifiedMTI}$). The key properties relating to the pipe and corrosion geometry, material properties, loadings, and the estimated burst pressures from the finite element analysis (FEA) results are used to generate NLRM and ANN models for each corrosion defect shape, resulting in seven NLRM and seven ANN models. The performances of the 14 ML models are tested using normalized real ILI data as illustrated in Fig. 4 and explained in the following sections.

4.1. Finite element methods

The static non-linear finite element burst models of pipelines with interacting corrosion defects using the features of 25 MTI test samples are summarized in Table 1, incorporating the seven defect shapes from Fig. 3. These models are developed using ANSYS workbench 2020, resulting in a total of 175 FEA models. A pipe length of 6D greater than the minimum requirement of 5D by British Standards Institution (BSI) recommendation 7910 (British Standards Institution, 2005) is used to fully highlight the stress distribution and deformations in the pipeline sections. A quarter or half pipe is simulated for test samples (TS) with symmetric layout of metal loss defects in the cylindrical pipe to reduce model computational time, and a full pipe was modelled for those with unsymmetrical corrosion defect colony configuration as displayed in Fig. 5. These models utilized a SOLID187 element type, which is a 3 dimensional tetrahedral structural solid with features to fully illustrate the plasticity effects of the pipe material (ANSYS Manual, 2009). The mesh densities at the corroded area are increased and convergence

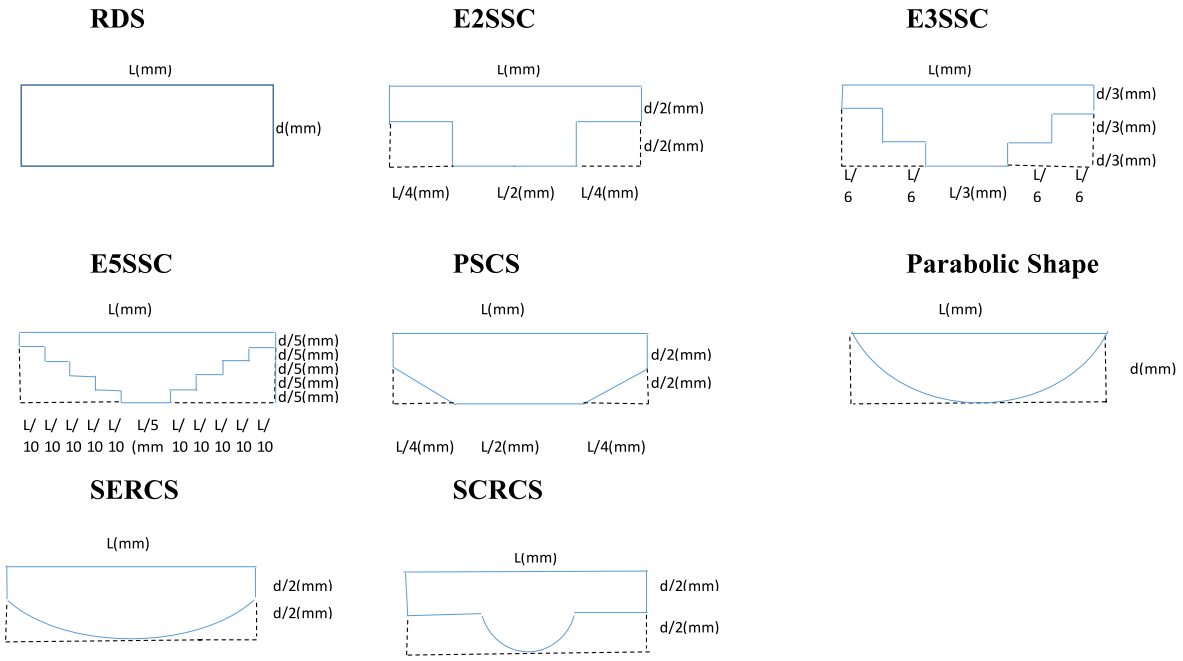

Fig. 3. Corrosion defect shapes.

Table 3
Corrosion defect shape factors.

Defect Shape	RDS	PS	SERCS	E2SSC	E3SSC	E5SSC	PSCS	SCRCS
Defect Shape Factor (S_F)	1.00	0.67	0.89	0.75	0.67	0.60	0.88	$[0.5 + (\frac{1}{16L}\pi d)]$

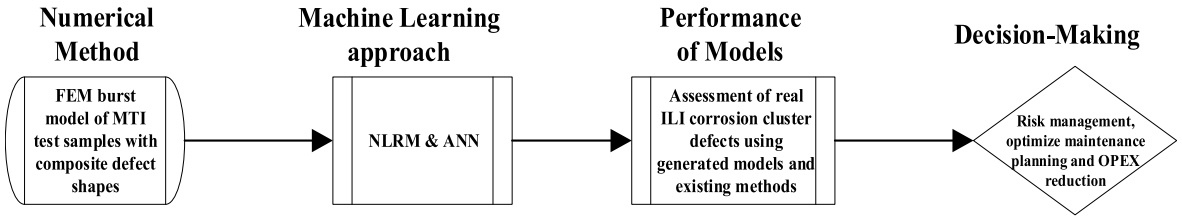

Fig. 4. Flow diagram of deterministic assessment of pipeline interacting corrosion defects.

studies are performed to obtain the optimum mesh density. The stress concentration areas due to sharp ends or corners at the corroded areas are minimized by introducing a fillet with a radius of 0.05 mm in the model geometry.

The pipeline properties are created using API 5L ×80 and API 5L ×70 grade carbon steel pipeline. The isotropic elastic properties (i.e., Young's modulus of elasticity and Poisson's ratio), density, true stress-plastic strain properties derived from De Andrade et al. (de Andrade and Benjamin), Yanfei et al. (Chen et al., 2015), Lee et al. (2018), tensile strength properties from Table 1 and Ramberg-Osgood formulation to cater for multilinear hardening of the pipes are specified and assigned to the pipeline. The symmetric faces of corroded area are restrained from displacing in the longitudinal and circumferential direction to create plain strain settings. To prevent the pipeline from expanding and contracting in the longitudinal direction, the end of the pipe away from the corroded area is restrained. The node at the pipe end farthest from the corroded section is fixed to prevent rigid body model of the model as illustrated in Fig. 6. The internal pressure is applied incrementally by means of the ANSYS ramped function in a ratio of 1 s to 1 MPa on the internal surface of cylindrical shaped pipe.

The plastic failure pressures are identified by examining internal pressure at the timestep when the equivalent von Mises stress through the thickness of the corroded areas exceeds the elastic deformation region's yield strength and reaches the true ultimate tensile strength at the corroded region of the pipe as shown in Fig. 7.

4.2. Finite element method validation

The FEM predicted failure pressures of the multiple interacting pipeline corrosion defects with RDS are validated with the MTI experimental burst pressures ($P_{b.EXP}$) and those with the proposed shapes are validated using modified MTI burst pressure ($P_{f.\ ModifiedMTI}$). The modified MTI burst pressure is obtained by introducing the derived defect shape factor (S_F) from Table 3 in equation (1) to account for the metal loss defect profile, in the absence of experiments for these shapes.

$$P_{f.ModifiedMTI} = UTS \times \left(\frac{2t}{D-t}\right) \times \frac{\left(1 - \left(S_F \times \frac{d_c^g}{t}\right)\right)}{\left(1 - \left(S_F \times \frac{d_c^g}{t}\right) \times \frac{1}{M_c^g}\right)} \quad (1)$$

where UTS is the ultimate tensile strength, t is the pipeline wall thickness, D is the outer diameter, d_c^g is the effective corrosion cluster depth

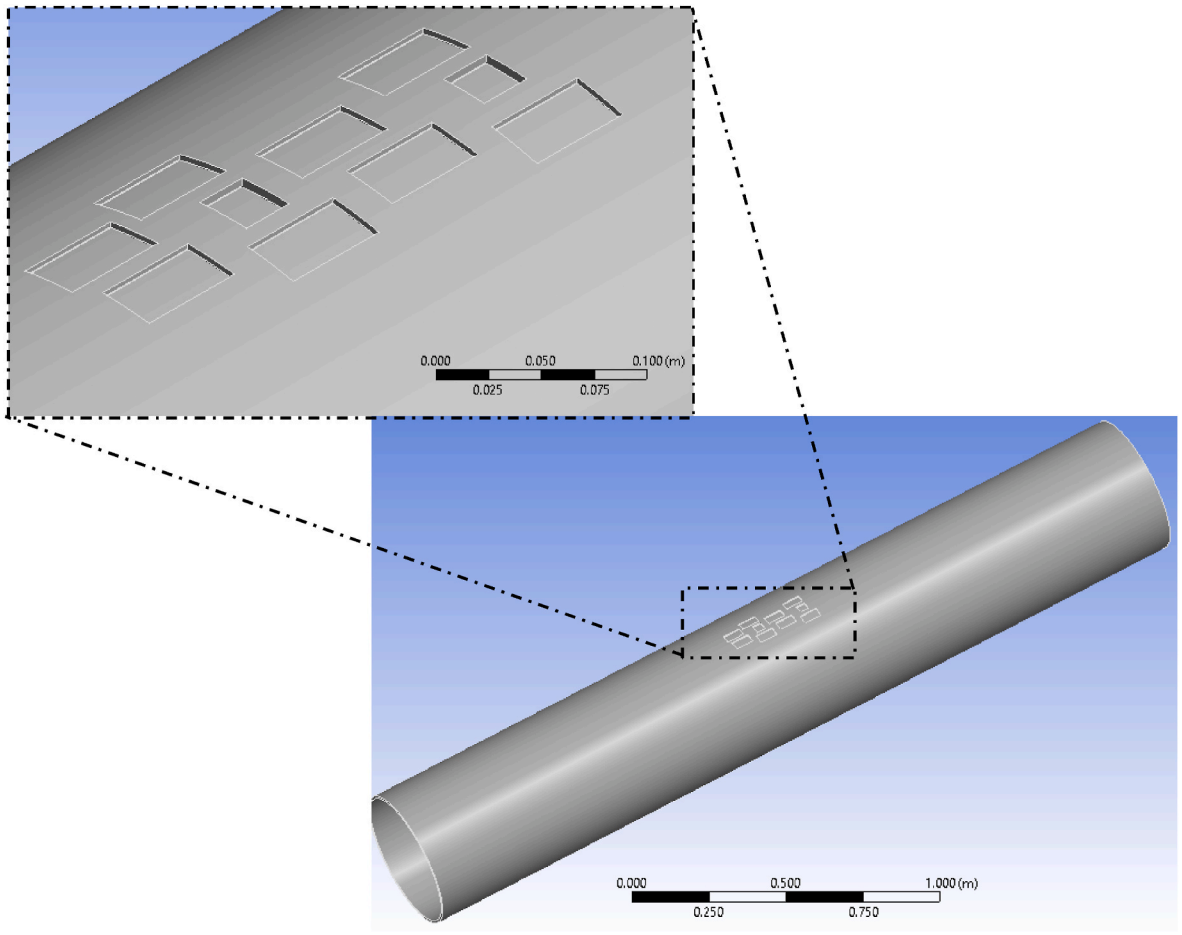

Fig. 5. A typical configuration of longitudinally and circumferentially interacting corrosion defects in pipe test sample 27.

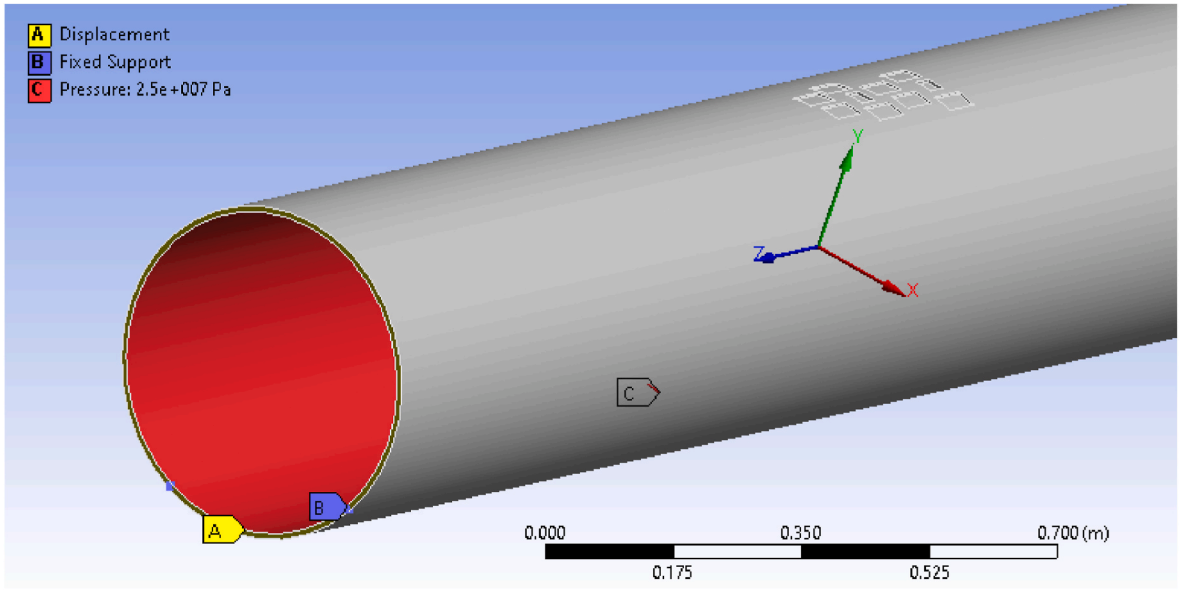

Fig. 6. Boundary conditions and loadings on pipe burst model.

and M_c^g is the bulging factor. The results from the validation of the RDS corrosion cluster are presented in Table 4. The total absolute mean deviation (TAMD) of the FEM predicted failure pressure from the experimental burst pressure is 2.025%, indicating the acceptability of the FEM burst models. Notably, the TAMD of the predicted FEA failure pressure of the corroded pipe with the other shapes aside the RDS are less than 2.152% from the estimated modified MTI burst pressure.

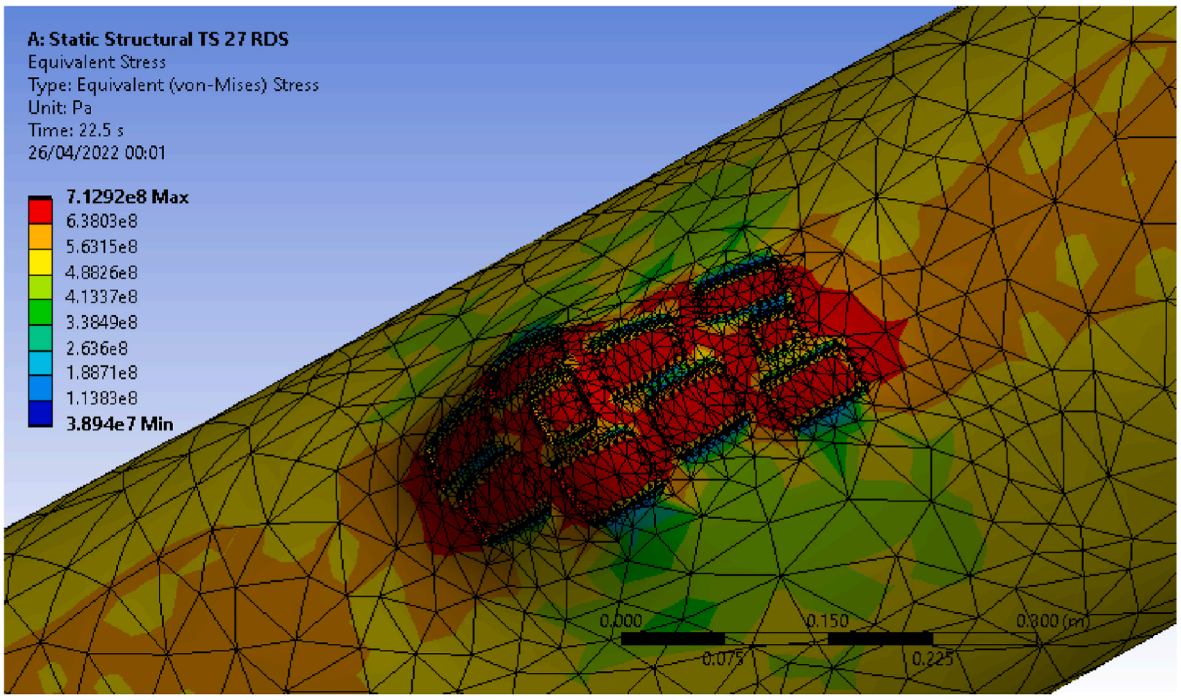

Fig. 7. Damaged FEA burst model.

Table 4
Comparison of FEM predicted failure pressure and experimental burst pressure-for RDS corrosion.

No.	Test Sample	FEM Predicted Failure Pressure (MPa)	Experimental Burst Pressure (MPa) (Benjamin et al., 2007, 2016b).	Percentage difference (%)
1	3	20.400	20.310	0.443
2	4	21.600	21.140	2.176
3	5	21.120	20.870	1.198
4	6	19.000	18.660	1.822
5	7	19.200	18.770	2.291
6	9	23.400	23.060	1.474
7	10	23.700	23.230	2.023
8	11	21.670	21.260	1.929
9	12	20.400	20.160	1.190
10	15	23.917	24.000	−0.346
11	16	23.572	23.400	0.735
12	17	21.423	21.200	1.052
13	18	22.800	22.700	0.441
14	19	23.500	23.300	0.858
15	20	21.100	20.800	1.442
16	21	22.778	22.600	0.788
17	22	20.500	20.300	0.985
18	23	21.800	21.500	1.395
19	24	21.600	20.500	5.366
20	25	21.400	19.900	7.538
21	26	21.200	19.800	7.071
22	27	22.500	21.300	5.634
23	28	23.400	23.200	0.862
24	29	23.600	23.400	0.855
25	30	21.250	21.100	0.711
Total Absolute Mean Deviation (TAMD)%				**2.025**

4.3. Supervised machine learning

Machine Learning (ML) methods employ statistical processes to uncover patterns in pre-processed data to derive critical features. There are three types of machine learning approaches namely supervised ML, unsupervised ML, and reinforcement learning. Supervised machine learning methods are usually applied to well-defined problems with known input variables referred to as predictors and an estimated response variable. This can be a classification or regression problem depending on the nature of the predictor variables and target response variables. Unsupervised ML methods seek to discover relationships for a system with only known predictor variables and reinforcement learning tends to unearth patterns related to reward and punishment indicators (Mirjalili et al., 2020).

Categorical ML methods such as NLRM and ANN methods can be used to further reduce the simulation computational time by deriving patterns from key features of interacting corrosion defects in pipelines and the estimated burst pressures to generate models for future applications (Fig. 8). These are achieved by training, testing, and validating the MATLAB learning algorithms on the developed dataset from the FEA comprising of key geometric and material properties as the predictors and the predicted FEA failure pressure as the target response variable.

In this paper, the NLRM is used to derive a relationship between the physical properties and the target failure pressure due to the non-linear behaviour of the interacting corroded defects. The Hougen-Watson model requirement by Douglas et al. (Douglas and Bates, 2007) by utilizing three predictors and three target variables is used to derive a simple but accurate correlation. Unlike the analyses by Silva et al. (2007) and Xu et al. (2017), this study incorporates the pipe material flow stress properties and defect shape factor that control the plastic deformation failure of carbon steel pipelines. Furthermore, the variability of corrosion defect profiles based on real inspection information is also implemented in developing the predictors. It is to be noted that the predictors in this analysis are constrained to three variables to prevent the issue of dimensionality, which was identified by Lu et al. (2021) as a major challenge in developing data-driven ML models for failure pressure prediction of corroded pipelines. The essential properties captured as the predictors are a ratio of effective defect depth of metal loss to pipe wall thickness, the plastic flow stress that depends on the pipe material UTS, and a unitless parameter relating to pipe bulging factor, longitudinal and circumferential defect spacing as shown in equations (3)–(5). The predicted pipeline pressure by numerical methods ($P_{f.FEM}$) and two unity responses are set as the output targets. The S_L of interacting corrosion can be investigated by setting S_C to unity, and varying S_L and vice-versa. The regression analysis is performed by changing the beta points till the root mean squared error (RMSE) and

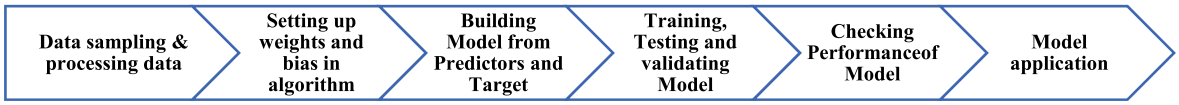

Fig. 8. Process flowchart of supervised ML.

regression coefficient of determination, R-squared value is acceptable. The R-squared value quantifies the relationship between outputs and targets whiles the RMSE is the rate of the mean error measure between the initial outputs and predicted target values. An R-squared value of one indicates a good relationship, and zero shows a random relationship (Mirjalili et al., 2020). The derived model to predict the pipeline failure pressure for all the 8 shapes ($P_{f.NLRM}$) is shown in equation (2).

$$P_{f.NLRM} = [(b_1 x_2) - (x_3 / b_5)] / [1 + (b_2 x_1) + (b_3 x_2) + (b_4 x_3)] \quad (2)$$

where b_1, b_2, b_3, b_4 and b_5 are the estimate coefficients from the non-linear regression results.

$$x_1 = S_F \bullet \left(\frac{d}{t}\right) \quad (3)$$

$$x_2 = UTS \bullet \left(\frac{2t}{D-t}\right) \quad (4)$$

$$x_3 = \left(\frac{|s_L|}{|s_c|} \bullet \frac{L^2}{Dt}\right) \quad (5)$$

ANNs are feed forward classification networks as shown in Fig. 9 that use known predictors and expected outcomes to derive a relationship model by using synaptic weights and learning process (de Andrade and Benjamin). In this model, the NLRM predictors and targets defined above are also used for the ANN model. The neural network employs a three-layer feed-forward structure with ten neurons in the hidden layer (five neurons are shown in Fig. 9 for demonstrative purposes) to solve the generated input-target response data created in the matrix row. The datasets are trained using the Levenberg-Marquardt backpropagation algorithm, which uses a short processing time till regression' R squared value and mean squared error (MSE) are acceptable. A good correlation is achieved by using 60% of the dataset for training, 20% for validation, and 20% for testing. Hence, a total of 175 datasets are used, resulting in 105 data points for training, 35 datasets for validation, and 35 datasets for testing.

The acceptable generated models are stored for future applications on the 15 severe corrosion clustered defect areas (CCDA) identified by ILI to estimate the pipeline failure pressure for the ANN and NLRM ($P_{f.\,ANN}$ and $P_{f.\,NLRM}$) due to the corrosion cluster. The predictors from the normalized ILI information used for evaluating the developed ML methods are presented in Table 5. The predicted pipeline failure pressures from the ANN ($P_{f.\,ANN}$) and NLRM ($P_{f.\,NLRM}$) are compared with the predicted pipeline failure pressure of existing assessment methods (such as the DNV ($P_{f.DNV}$) and MTI ($P_{f.MTI}$)) and the observations are discussed in section 5.2.

5. Results and discussion

5.1. Finite element models

A sample size of 25 RDS burst models from the MTI's full scale burst

Table 5
Predictors from ILI data for performance testing of NLRM and ANN Models.

Severe Corrosion Clustered Defect Areas (CCDA)	1st Predictor Term	2nd Predictor term	3rd Predictor term
	$S_F \bullet \left(\frac{d}{t}\right)$	$UTS \bullet \left(\frac{2t}{D-t}\right)$	$\left(\frac{\lvert s_L\rvert}{\lvert s_c\rvert} \bullet \frac{L^2}{Dt}\right)$
CCDA 1	0.4891	25.45	7.6005
CCDA 2	0.6124	25.45	2.1708
CCDA 3	0.4046	25.45	4.1226
CCDA 4	0.4894	25.45	6.8615
CCDA 5	0.4995	21.96	2.8546
CCDA 6	0.5195	21.96	26.7999
CCDA 7	0.3745	21.96	8.8956
CCDA 8	0.4353	25.45	5.0375
CCDA 9	0.5332	25.45	46.2016
CCDA 10	0.4262	25.45	24.6484
CCDA 11	0.3381	21.96	8.3227
CCDA 12	0.2657	21.96	1.7954
CCDA 13	0.3010	21.96	5.1634
CCDA 14	0.2300	25.45	0.4131
CCDA 15	0.2605	25.45	8.7491

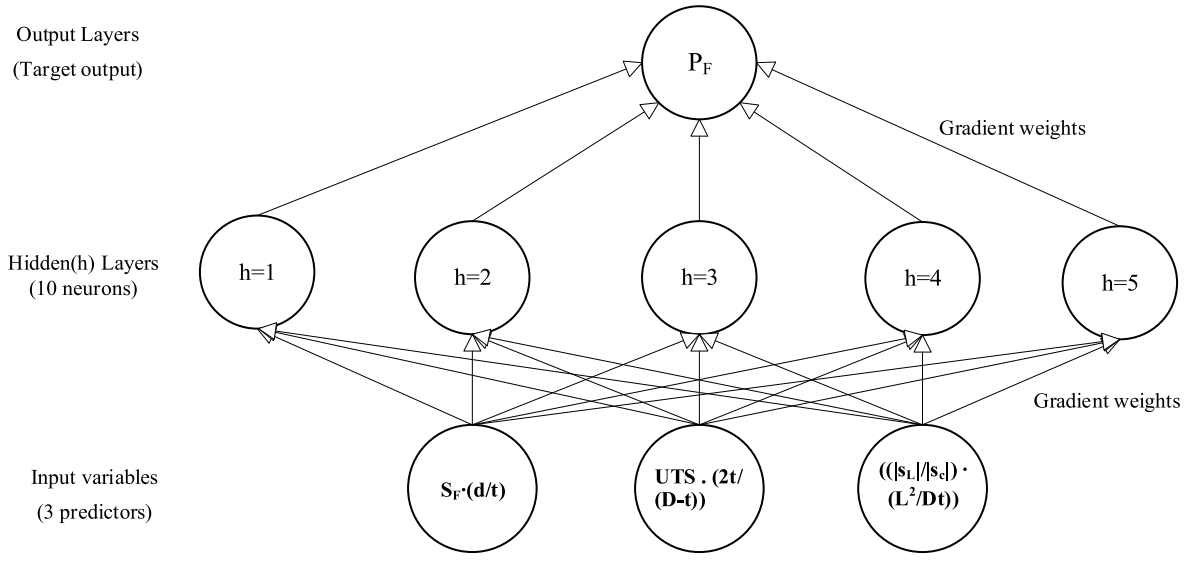

Fig. 9. Structure of the ANN method.

test using the same features in terms of the configuration of longitudinally and circumferentially interacting corrosion defects and material properties are numerically modelled. The estimated pipeline failure pressures from the finite element analysis are compared with the experimental burst pressures and relevant approaches in the literature for evaluating interacting corrosion defects, as illustrated in Fig. 10 and Table 6. In Fig. 10 and Tables 6 and it is worth noting that the burst pressure prediction by the finite element methods for the RDS samples yielded a slender margin of failure pressure overestimation with total absolute mean deviation of 2.025% from the experimental burst pressures, standard deviation of 2.084% and pressure prediction percent range from +7.538% to −3.460%. The existing approaches such as the DNV, MTI, Modified ASME B31G and the RSTRENG effective area provided conservative failure pressure estimation results that necessitate the need to improve the accuracy and model simulation time. A safety factor can be employed to transform or calibrate the predicted FEA results to underestimate the burst pressure to avoid unexpected pipeline failure during operations for all cases where the predicted pressure is more than experimental failure pressure.

The DNV approach for interacting metal loss defects produced an underestimated failure pressure with trendlines beneath the MTI prediction resulting in a total absolute mean deviation of 17.280% from the experimental burst pressures, standard deviation of 9.864% and pressure prediction percent range from +2.5% to −29.648%. The trendlines for the Modified ASME B31G and RSTRENG methods are further below the DNV predictions of the test samples considered, reechoing their conservatism with a total absolute mean deviation of 27.034% and 24.004% respectively.

To further investigate the effect of the variations in corrosion defect profile on the burst pressure of a corroded API 5L ×80 and ×70 pipe, an additional 150 FEA burst models are developed using the same interacting corrosion cluster configurations, material properties and environmental loadings but with the six improved corrosion defect shapes, resulting in 25 burst models per defect shape. The pipeline failure pressures from the FEA studies are compared with the proposed Modified MTI approach based on the defect shape factors as demonstrated in Fig. 11, Fig. 12, and Table 7. It is observed from predicted failure pressures that as the defect shape factor decreases and the volume of metal loss decreases, the pipeline fails at a higher pressure at the corrosion site by plastic deformation. The pipeline fails when maximum Von Mises equivalent stress reaches the flow stress of the pipeline material, which is located between the specified minimum yield strength and the ultimate tensile strength. Therefore, samples with same or approximately equal defect shape factor behave similarly as seen in the parabolic shaped (PS) sample and E3SSC with defect shape factor of 0.67 as well as the SERCS and E5SSC models with a defect shape factor of about 0.9.

Table 6
Total absolute mean error of the predicted burst pressure from the experiment test results for the RDS test samples.

Burst Pressure Prediction method	FEA	MTI	DNV	Modified ASME B31G	RSTRENG Effective Area
Total absolute mean deviation (%)	2.025	4.744	17.280	27.034	24.004
Maximum and Minimum positive deviation (%)	7.538, 0.441	6.200, 0.400	2.500	–	–
Maximum and Minimum negative deviation (%)	−0.346	−16.406, −2.660	−29.648, −5.66	−42.180, −1.100	−32.906, −8.800
Standard deviation	2.084	6.283	9.864	11.644	5.638

In Figs. 11 and 12, the experimental burst pressure with RDS for almost all the test samples is the lowest, followed closely by the RDS numerical burst model with a total mean deviation of 2.025%. The total mean deviation percent and standard deviation for the FEM models with the improved defect shapes from the modified MTI do not exceed 2.152% and 2.768 respectively as indicated in Table 7.

Significantly, the total mean deviation of the finite element models of the corroded pipes with improved shapes SERCS, PSCS, E2SSC, E3SSC, PS and E5SSC from the full-scale burst tests using rectangular defect shapes are 4.272%, 4.882%, 6.603%, 8.269%, 8.874% and 9.891% respectively as presented in Table 8.

These deviations from the RDS confirm the defect shape factor – predicted pipeline failure pressure relationship that contributes to the non-linear behaviour of interacting corrosion in pipelines. The pipeline

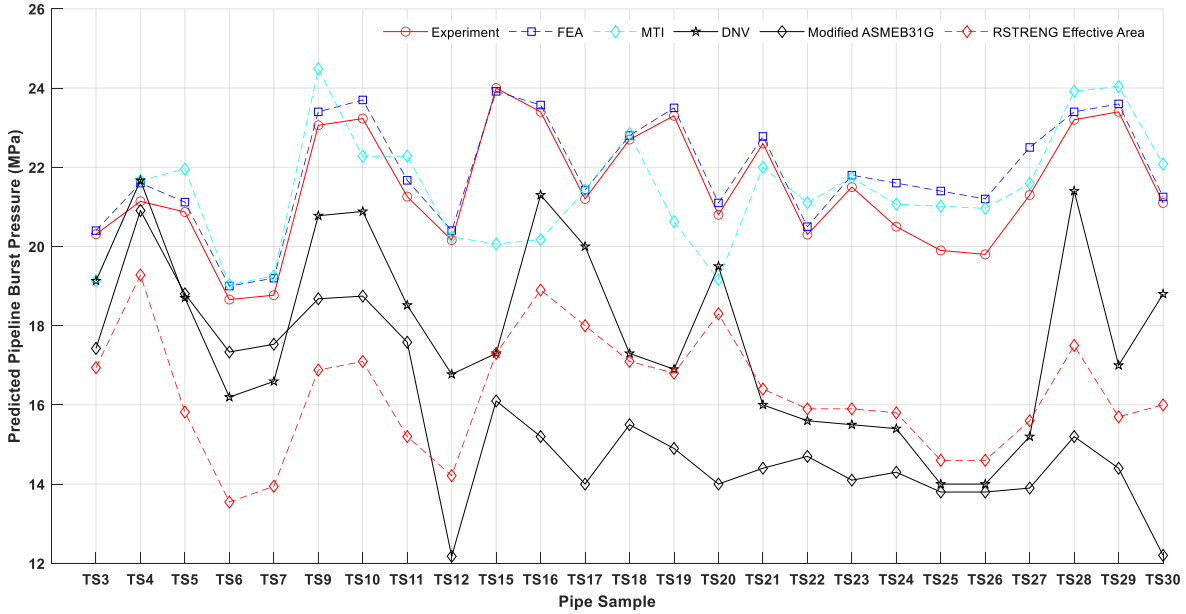

Fig. 10. Predicted pipeline failure pressure of RDS test samples using FEA, experiment, and other existing methods.

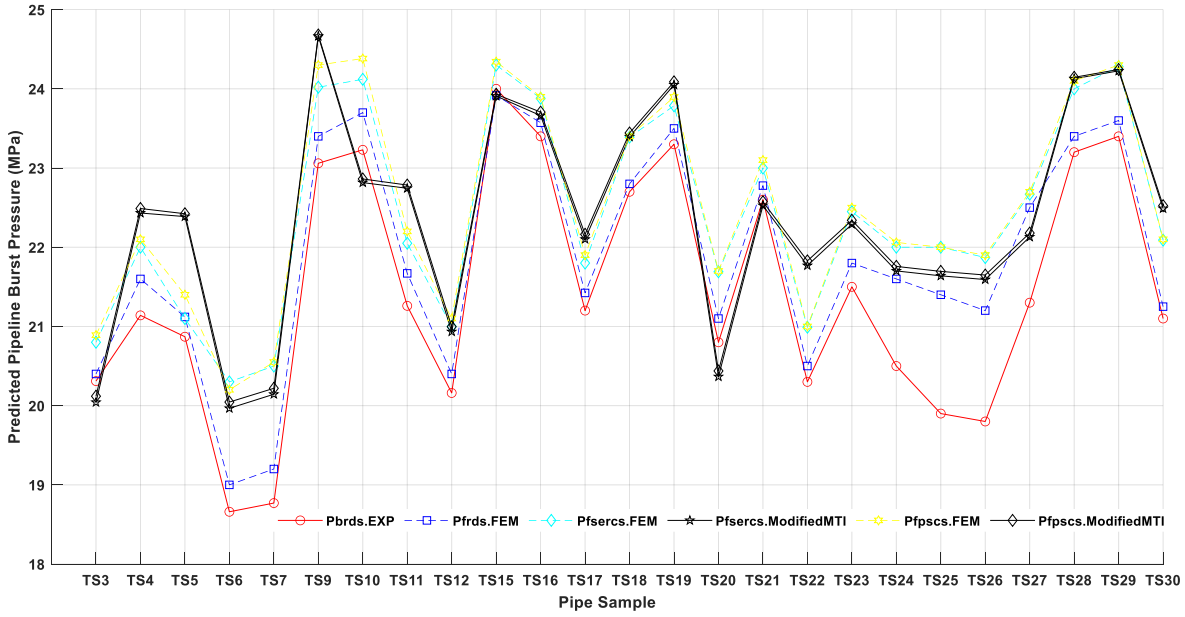

Fig. 11. Predicted pipeline failure pressure of RDS, SERCS and PSCS test samples using FEA, experiment, and Modified MTI method.

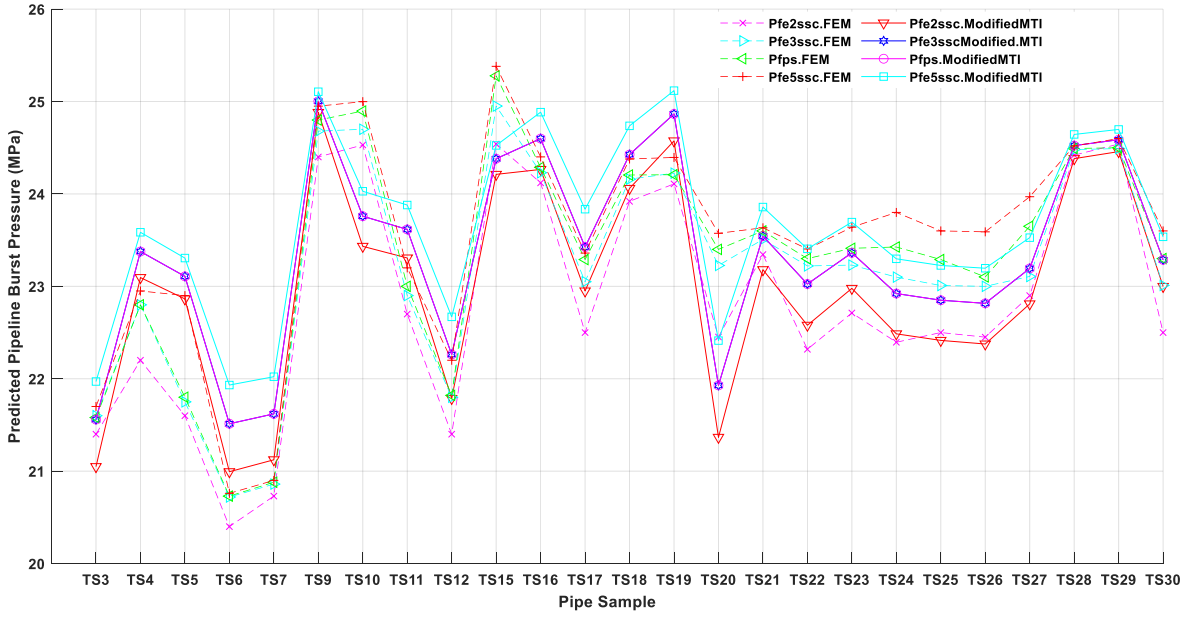

Fig. 12. Predicted pipeline failure pressure of E2SSC, E3SSC, E5SSC and PS test samples using FEA, and Modified MTI methods.

Table 7
Total absolute mean deviation of the FEM predicted burst pressure against the benchmark for all shapes.

Burst Pressure prediction per defect shape profile	Pfsercs	Pfpscs	Pfe2ssc	Pfe3ssc	Pfps	Pfe5ssc
Total absolute mean deviation (%)	2.152	2.004	1.817	1.884	2.032	2.093
Maximum and Minimum positive deviation (%)	6.500, 0.217	6.647, 0.230	5.081, 0.157	5.921, 0.196	6.714, 0.056	5.181, 0.270
Maximum and Minimum negative deviation (%)	−5.749, −0.018	−4.564, −0.183	−5.529, −0.405	−5.875, −0.155	−5.659, −0.126	−5.346, −0.009
Standard deviation	2.768	2.636	2.332	2.457	2.748	2.600

fails at a higher pressure as the defect shape factor decreases.

5.2. Non-linear regression and artificial neural networks models

The non-linear regression and ANN models are generated by training, testing, and validating with the predictors and validated FEA predicted failure pressure as described in section 3.3. The performance of the seven NLRM and seven ANN models are assessed with normalized real ILI data. In this paper, 15 severe clustered corrosion sites are selected from the ILI data and the results using the NLRM, and ANN

Table 8
Corrosion defect shape and deviation from experimental burst pressure of pipe samples with RDS.

Defect Shape	RDS	SERCS	PSCS	E2SSC	E3SSC	PS	E5SSC
Defect Shape Factor (S_F)	1.00	0.89	0.88	0.75	0.67	0.67	0.60
FEA model deviation from experimental burst pressure of pipe samples with RDS	2.025	4.272	4.882	6.603	8.269	8.874	9.891

model are presented in Figs. 13–15.

In Fig. 13, the predictions of the ANN model and NLRM follow closely to the MTI predictions for rectangular defect shaped corrosion for the 15 CCDA, yielding a total mean deviation of 1.479% and 6.502% respectively. The accurate prediction by the ANN model is evidenced by the R squared and the MSE of 0.9985 and 0.84235 respectively as shown in Table 9.

However, the failure pressure predictions from the DNV approach are underestimated for all the corrosion clusters considered with a total mean deviation of 26.019% from the MTI pipeline failure pressure prediction as presented in Fig. 13 and Table 10. This is mainly due to the translation of the interacting corrosion defects to a longitudinal and circumferential imaginary axis to compute the effective composite defect length and depth, which usually fails to account for the remaining wall thickness between the interacting pitting corrosion sites.

The trend relating to the defect shape factor and the predicted pipeline failure pressure as observed in the finite element results in Figs. 11 and 12 are also seen in Figs. 14 and 15. As the volumetric metal loss decreases, the pipeline fails at a higher pressure for a corroded pipeline with the same layout of interacting corrosion cluster defects. The trendline for the NLRM and ANN models for the ILI data follow closely to the predictions by the Modified MTI for the improved shapes. The ANN model for SERCS, PSCS and E2SSC defect shapes produces the best fit for the burst pressure for all the 15 corrosion cluster sites with a total absolute mean deviation of 1.8%, 2.4% and 3.1% from the modified MTI predictions respectively as seen in Fig. 14 and Table 10. The NLRM for the SERCS, PSCS and E2SSC defect shapes provide a TAMD not exceeding 7.3% from the Modified MTI. The trendline for the SERCS and PSCS samples with the defect shape factor of 0.89 and 0.88 respectively are similar as seen in Fig. 14. Therefore, for a corrosion site on the pipeline, the failure happens at a much higher stress for defect shapes that are E2SSC, followed by PSCS and marginally followed by SERCS.

Similarly, the trendline for the failure pressure prediction for the E3SSC and parabolic shaped defect sample by the NLRM and ANN Model exhibit same patterns due to the same defect shape factor of 0.67, providing a total absolute deviation not exceeding 7.3% and 2.87% respectively from their benchmark Modified MTI approach as shown in Fig. 15 and Table 10. The E5SSC with a defect shape factor of 0.6 has the smallest volumetric metal loss and the pipeline at the severe corrosion sites fails a much higher pressure than the other improved shapes, with a deviation of 3.1% and 7.1% from the Modified MTI predictions for the ANN model and NLRM respectively.

6. Conclusions

In an era of big data especially from intelligent pigging of long span pipelines, the need for computationally efficient modelling schemes to provide accurate and high precision burst pressure of pipelines with longitudinal and circumferential interacting corrosion cluster defects subjected to a net internal pressure has been established. This was accomplished by developing validated FEA models of API 5L ×70 and API 5L ×80 pipes with interacting metal loss defects combined with Artificial Neural Network and Non-Linear Regression Models. Furthermore, six improved metal loss defect shapes are proposed in the finite element models to investigate the non-linear performance of interacting corrosion defects, resulting in 150 FEA models to accommodate for the complex corrosion profiles captured by pipeline intelligent pigging tool.

From the structural integrity assessment of pipeline corrosion cluster defects, the following inferences were noted. Firstly, although the FEA computations are generally time consuming, they can be used to generate the machine learning database appropriate to investigate the general patterns in interacting corrosion, with acceptable deviation from expensive experiments. In this study, the anticipated FEA pipeline failure pressure using twenty-five MTI test samples with ideal rectangular defect shapes has a total absolute mean deviation of 2.03% from the experimental burst pressure. This mean deviation is lesser than the burst pressure prediction obtained from the conservative MTI, DNV,

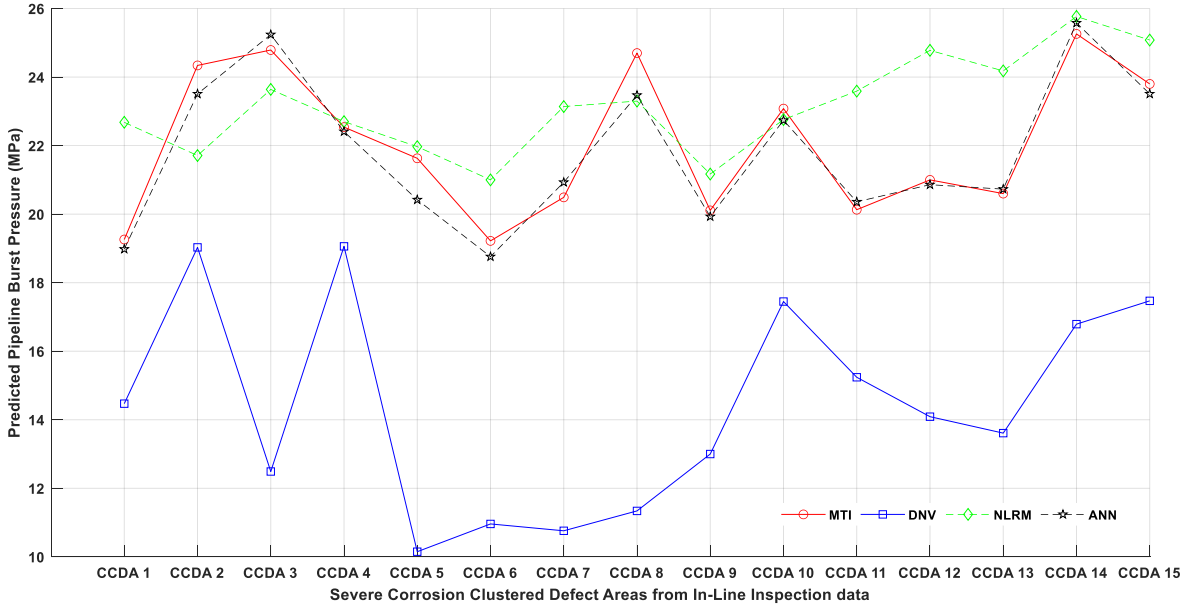

Fig. 13. Predicted pipeline failure pressure of normalized RDS ILI data using NLRM and ANN model.

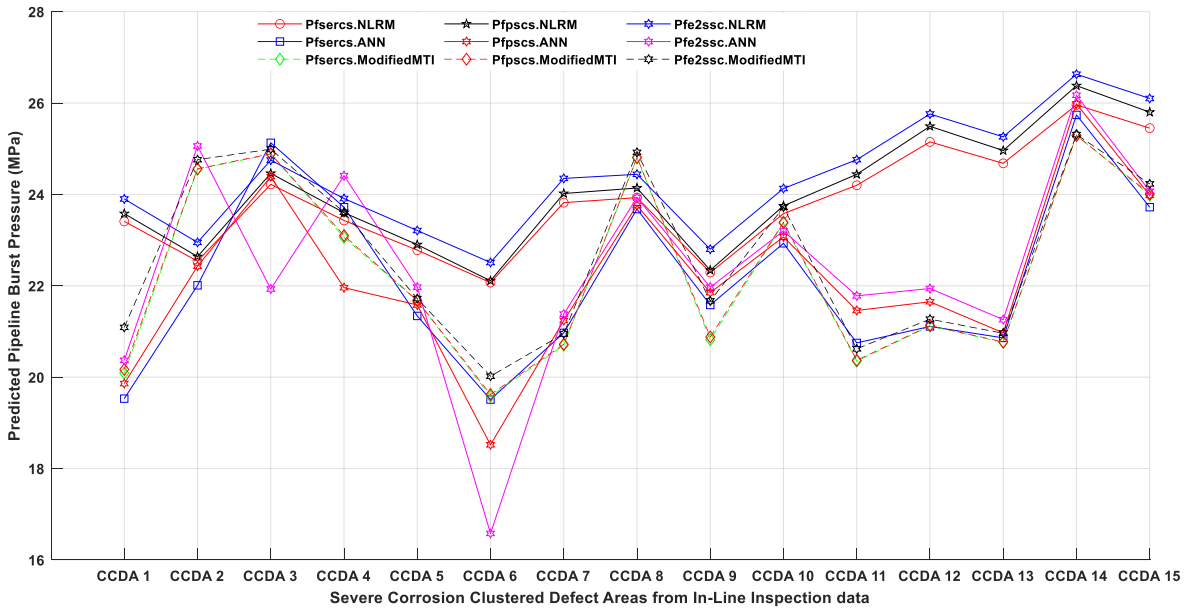

Fig. 14. Predicted pipeline failure pressure of normalized ILI data with improved metal loss defect shapes (SERCS, PSCS, E2SSC) using NLRM and ANN model.

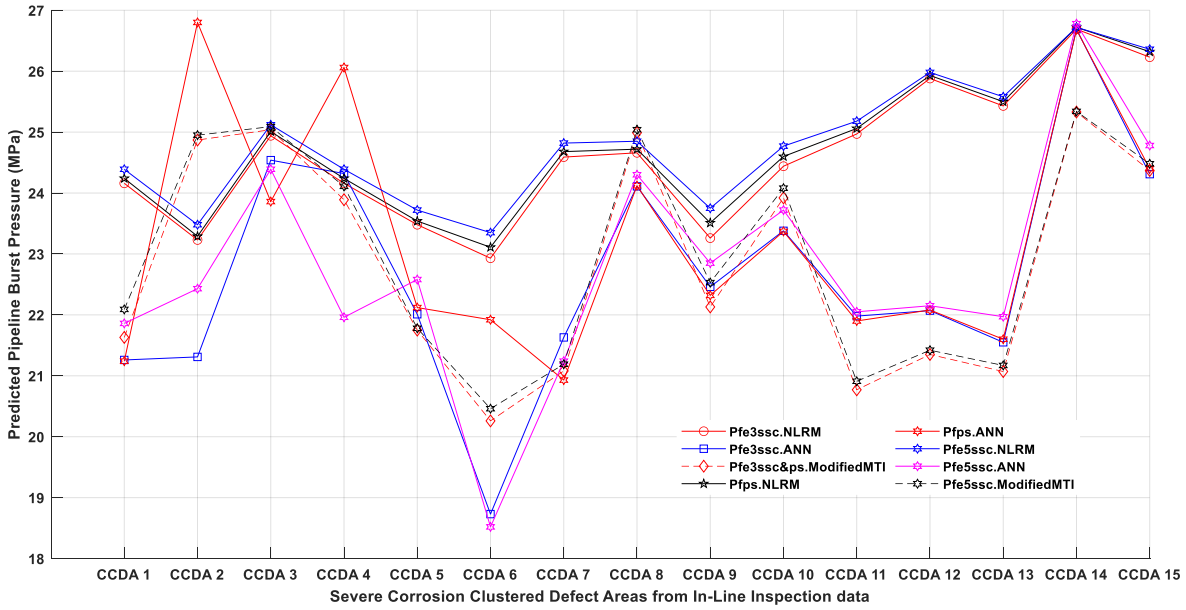

Fig. 15. Predicted pipeline failure pressure of normalized ILI data with improved metal loss defect shapes (E3SSC, PS, E5SSC) using NLRM and ANN model.

Table 9
Performance of ANN model.

ANN Model	RDS	SERCS	PSCS	E2SSC	E3SSC	PS	E5SSC
Coefficient of determination, R	0.9985	0.9991	0.99913	0.99944	0.99953	0.99925	0.99934
Mean Squared Error, MSE	0.84235	0.51697	0.31046	0.25699	0.029515	0.097489	0.22258

RSTRENG Effective Area and ASME B31G semi-empirical formulations which produce a total mean deviation of 4.74%, 17.28%, 24.00% and 27.03% respectively. Significantly, the total mean deviation percent for the FEA models with the improved defect shapes from the proposed Modified MTI formulations in equation (1) does not exceed 2.2%.

The ANN models proved to be more efficient than the NLRM correlation in the assessment of interacting corrosion defects in pipelines. The TAMD from the modified MTI approach for the neural network model and NLRM for the RDS samples from the real inspection information are 1.5% and 6.5% respectively. Notably, the ANN Models and NLRM for the severe corrosion cluster defect data from the ILI data produce pipeline failure pressure predictions with TAMD not beyond 3.1% and 7.3%. It is worth noting that the results from FEM models and the predictions of the NLRM and ANN model show a common trend of the behaviour of corroded pipeline in relation to the defect shape factor, where for the same conditions, as the volume or cross-sectional area of corroded

Table 10
Performance of developed NLRM and ANN Models for all defect shapes.

Burst Pressure prediction for all metal loss defect shape		Pfrds	Pfsercs	Pfpscs	Pfe2ssc	Pfe3ssc	Pfps	Pfe5ssc
NLRM	**Total absolute mean deviation (%)**	6.502	6.950	7.333	7.088	7.065	7.308	7.128
	Maximum and Minimum positive deviation (%)	17.97, 0.73	19.09, 0.90	20.60, 1.51	21.11, 1.28	21.23, 1.17	21.46, 1.49	21.31, 0.09
	Maximum and Minimum negative deviation (%)	−10.81, −1.39	−8.16, −2.68	−7.82, −2.71	−7.33, −0.94	−6.59, −0.40	−6.36, −0.15	−5.89, −0.77
	Standard deviation	9.43	9.02	9.15	8.88	8.72	8.74	8.61
ANN Model	**Total absolute mean deviation (%)**	1.479	1.788	2.374	3.121	2.772	2.870	3.086
	Maximum and Minimum positive deviation (%)	2.12, 0.63	3.62, 0.47	5.34, 0.95	5.59, 1.21	5.80, 1.18	9.10, 0.14	5.67, 0.24
	Maximum and Minimum negative deviation (%)	−5.57, −0.54	−10.33, −0.06	−8.68, −0.13	−17.22, −0.65	−14.31, −0.22	−4.72, −0.68	−10.11, −1.03
	Standard deviation	2.315	3.465	3.969	6.182	5.174	4.366	5.260
DNV Method	**Total absolute mean deviation (%)**	26.019						
	Maximum and Minimum positive deviation (%)	–						
	Maximum and Minimum negative deviation (%)	−54.10, −15.44						
	Standard deviation	12.210						

materials increases, the pipeline failure pressure reduces. Given an established corrosion defect shape by an In-line Inspection tool, the proposed composite shapes give the option to select an appropriate defect shape factor for performance assessment purposes. For example, if the corroded area is 75% of an equivalent rectangular shape defined by the maximum defect length and depth, the composite shape E2SSC is the best shape for assessment. Hence, the outcomes from this assessment with different shapes afford an opportunity to critically examine corrosion colonies in a pipeline to provide reliable estimates associated with the actual defect profiles of ILI tools to make informed reliability and integrity decisions in the areas of maintenance, operations, and decommissioning planning. In this paper, the uncertainties relating to geometric and material properties, corrosion growth rate and loading conditions are not considered and will be investigated in the next stage of this research. Also, only discrete defect shape factors are considered but a continuous defect shape function will be explored in the future to account for the defect profile variability.

CRediT authorship contribution statement

Abraham Mensah: Methodology, Software, Validation, Investigation, Writing – original draft, preparation, Funding acquisition. **Srinivas Sriramula:** Conceptualization, Supervision, Writing – review & editing, Resources, Project administration.

Declaration of competing interest

The authors declare the following financial interests/personal relationships which may be considered as potential competing interests: Abraham Mensah reports a relationship with Ghana National Gas Company that includes: employment.

Data availability

The authors do not have permission to share data.

Acknowledgements

The first author would like to thank the Ghana National Petroleum Corporation (GNPC) Foundation for funding the PhD studies at the University of Aberdeen. The first author also acknowledges the research support from Net Zero Technology Centre and University of Aberdeen through their partnership in the UK National Decommissioning Centre.

References

Amaya-Gómez, R., Sánchez-Silva, M., Muñoz, F., 2016. Pattern recognition techniques implementation on data from In-Line Inspection (ILI). J. Loss Prev. Process. Ind. 44, 735–747.
Amaya-Gómez, R., Sánchez-Silva, M., Muñoz, F., 2019. Integrity assessment of corroded pipelines using dynamic segmentation and clustering. Aug 1 Process Saf. Environ. Protect. 128, 284–294.
ANSYS Manual, 2009. Theory reference for the mechanical APDL and mechanical applications. Release 120.
ASME B31G, 2012. Manual for Determining the Remaining Strength of Corroded Pipelines. Supplement to ASME B31 Code for Pressure Piping.
Benjamin, A.C., Freire, J.L.F., Vieira, R.D., 2007. Part 6: "Analysis of pipeline containing interacting corrosion defects. May Exp. Tech. 31 (3), 74–82.
Benjamin, A.C., Freire, J.L.F., Vieira, R.D., Cunha, D.J.S., 2016a. Interaction of corrosion defects in pipelines - Part 1: fundamentals. Int. J. Pres. Ves. Pip. 144, 56–62.
Benjamin, A.C., Freire, J.L.F., Vieira, R.D., Cunha, D.J.S., 2016b. Interaction of corrosion defects in pipelines – Part 2: MTI JIP database of corroded pipe tests. Int. J. Pres. Ves. Pip. 145, 41–59.
British Standards Institution, 2005. European Committee for Standardization. Guide to Methods for Assessing the Acceptability of Flaws in Metallic Structures. British Standards Institution, p. 297.
Chen, Y., Zhang, H., Zhang, J., Li, X., Zhou, J., 2015. Failure analysis of high strength pipeline with single and multiple corrosions. Feb 15 Mater. Des. 67, 552–557.
Cosham, A., Hopkins, P., Macdonald, K.A., 2007. Best practice for the assessment of defects in pipelines – corrosion. Oct Eng. Fail. Anal. 14 (7), 1245–1265.
de Andrade EQ, Benjamin AC., "Finite element modelling of the failure behavior of pipelines containing interacting corrosion defects." In: Proceeding of the ASME 25th International Conference on Offshore Mechanic and Arctic Engineering, (Hamburg, Germany).
Det Norske Veritas, 2004. Recommended Practice, DNV-RP-F101. Corroded Pipelines [Online]. Available: http://www.dnv.com.
Douglas, M., Bates, Donald G. Watts, 2007. Nonlinear Regression Analysis and its Applications." No. 1. John Wiley and Sons Ltd.
EGIG, 2020. 11th Report of the European Gas Pipeline Incident Data Group (1970-2019) [Online]. Available. https://www.EGIG.eu.Doc. number VA 20.0432, 17th December 2020.
Grady, O., Thomas, J., Hisey, I., Kiefner, D.T., John, F., 1992a. Method for evaluating corroded pipe addresses variety of patterns. Oil Gas J. 12.
Grady, O., Thomas, J., Hisey, I., Kiefner, D.T., John, F., 1992b. Pressure calculation for corroded pipe developed (Part 2). Oil Gas J. 90.
Huang, Y., Qin, G., Hu, G., 2022. Failure pressure prediction by defect assessment and finite element modelling on pipelines containing a dent-corrosion defect. Ocean Eng. 266 https://doi.org/10.1016/j.oceaneng.2022.112875.
Lee, S.I., Lee, S.Y., Lee, S.G., Jung, H.G., Hwang, B., 2018. Effect of strain aging on tensile behavior and properties of API X60, X70, and X80 pipeline steels. Nov 1 Met. Mater. Int. 24 (6), 1221–1231.
Lo, M., Karuppanan, S., Ovinis, M., 2021. Failure pressure prediction of a corroded pipeline with longitudinally interacting corrosion defects subjected to combined loadings using FEM and ANN. Mar 1 J. Mar. Sci. Eng. 9 (3).
Lu, H., Xu, Z.-D., Iseley, T., Matthews, J.C., 2021. Novel data-driven framework for predicting residual strength of corroded pipelines. J. Pipeline Syst. Eng. Pract. 12 (4) https://doi.org/10.1061/(asce)ps.1949-1204.0000587.
Lu, H., Peng, H., Xu, Z.-D., Matthews, J.C., Wang, N., Iseley, T., 2022. A feature selection–based intelligent framework for predicting maximum depth of corroded pipeline defects. J. Perform. Constr. Facil. 36 (5) https://doi.org/10.1061/(asce)cf.1943-5509.0001753.
Lyons, C.J., Goodfellow, G.D., Haswell, J.V., 1962. UKOPA Pipeline Product Loss Incidents and Faults Report, 2018. Report Number: UKOPA/RP/19/002, February 2020.

Ma, Q., Tian, G., Zeng, Y., Li, R., Song, H., Wang, Z., et al., 2021. Pipeline In-Line Inspection Method, Instrumentation, and Data Management, vol. 21. Sensors. MDPI AG.

Mazumder, R.K., Salman, A.M., Li, Y., 2021. Failure risk analysis of pipelines using data-driven machine learning algorithms. Mar 1 Struct. Saf. 89.

Mirjalili, S, Faris, H, Aljarah, I., 2020. Evolutionary Machine Learning Techniques: Algorithms and Applications. Springer Nature Singapore eBook ISBN: 978-981-32-9990-0. https://doi.org/10.1007/978-981-32-9990-0.

Qin, G., Cheng, Y.F., 2021. A review on defect assessment of pipelines: principles, numerical solutions, and applications. Int. J. Pres. Ves. Pip. 191. Elsevier Ltd.

Silva, R.C.C., Guerreiro, J.N.C., Loula, A.F.D., 2007. A study of pipe interacting corrosion defects using the FEM and neural networks. Adv. Eng. Software 38 (11–12), 868–875.

Sun, M., Zhao, H., Li, X., Liu, J., Xu, Z., 2021. New evaluation method of failure pressure of steel pipeline with irregular-shaped defect. May 1 Appl. Ocean Res. 110.

U.S. Department of Transport PHMSA, 2020. Gas Distribution Significant Incidents Cause, 2005-2020". Data as of 18th March 2021. [Online]. Available: https://www.phmsa.dot.gov/.

Wang, Y., Li, R., Xia, A., Ni, P., Qin, G., 2023. An integrated modeling method of uncertainties: application-orientated fuzzy random spatiotemporal analysis of pipeline structures. Tunn. Undergr. Space Technol. 131 (Jan) https://doi.org/10.1016/j.tust.2022.104825.

Xu, W.Z., Li, C.B., Choung, J., Lee, J.M., 2017. Corroded pipeline failure analysis using artificial neural network scheme. Oct 1 Adv. Eng. Software 112, 255–266.